Modeling the Lux/AiiA Relaxation Oscillator

Christopher Batten

MIT Computer Science and Artificial Intelligence Laboratory

The Stata Center, 32 Vassar Street, Cambridge, MA 02139

This document describes a preliminary model for a Lux/AiiA Synchronized Relaxation Oscillator (LASRO), which uses the Lux quorum sensing positive feedback mechanism coupled with AiiA, an enzyme which actively degrades the acylhomoserine lactone (HSL) component of the positive feedback loop to create synchronized population level oscillations. Figure 1 illustrates the full system we are investigating. Essentially this is the standard Lux quorum-sensing system with the expression of AiiA coupled to the expression of LuxI.

A similar relaxation oscillator has been proposed which uses the λ bacteriophage cI repressor positive feedback loop and the RcsA protease for cI [2]. This system was later altered to use cII and $FtsH$ and extended to include a cell-to-cell signaling mechanism which theoretically enabled synchronized population level oscillations [4]. The LASRO system introduced in this document differs from these earlier proposals since it effectively integrates the oscillator and synchronization subsystems into a single system. The relaxation oscillator proposed by the summer students at the California Institute of Technology uses a significantly different negative feedback loop; a repressor protein is able to repress the same operator normally targeted by the positive feedback activator [5].

To gain some qualitative insight we will initially work under the *rapid equilibrium approximation*. This approximation assumes that that the timescale of protein-protein and protein-DNA interactions are significantly faster than the other chemical reactions and thus we can consider these protein reactions to be at equilibrium. We begin our analysis by examining a simple model for a bistable positive-feedback network. Insight into the bistability of this simple network will give us a better understanding of the relaxation oscillator's dynamics. We then self-couple this simple positive feedback network to derive a greatly
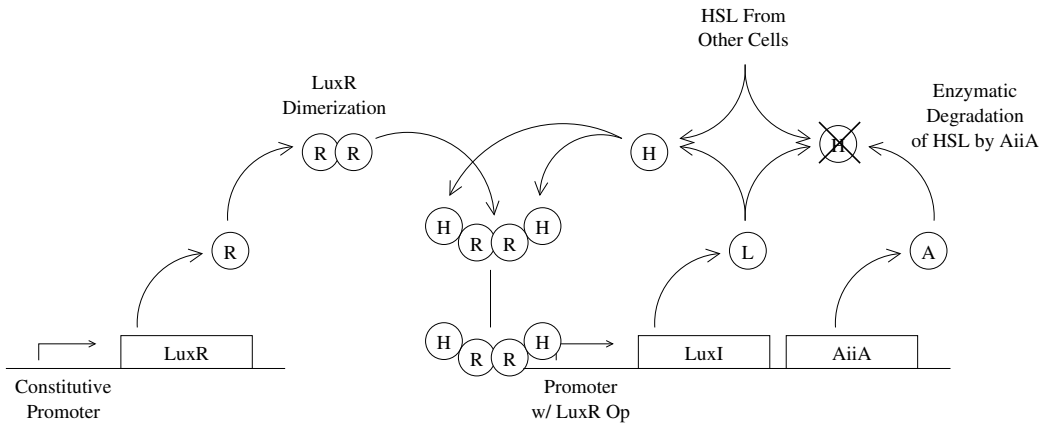

Figure 1: System Diagram for Lux/AiiA Synchronized Relaxation Oscillator
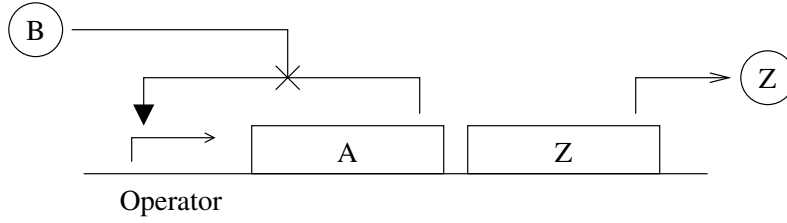
Figure 2: System Diagram for Bistable Positive-Feedback Network

(a)	Multimerization	$nA \rightleftharpoons A_n$	$K_1 = (A)^n/(A_n)$
(b)	Activation	$O + A_n \rightleftharpoons OA_n$	$K_2 = (O)(A_n)/(OA_n)$
(c)	Leakage	$O \rightarrow O + A + Z$	k_{leak}
(d)	Synthesis	$OA_n \rightarrow OA_n + A + Z$	k_{synth}
(e)	Protein Decay	$A \rightarrow$	k_{adeg}
(f)	Protein Decay	$Z \rightarrow$	k_{zdeg}
(g)	Decay of A by B	$A + B \rightarrow B$	k_{AB}

Table 1: Chemical Equations for LASRO Without Negative Feedback

simplified model of the full LASRO system. We examine how various parameters influence this simplified system's oscillatory behavior. We will then reconsider the rapid equilibrium approximation before investigating the simplified LASRO system with biologically plausible parameters. We conclude with one possible strategy for actually building the LASRO system.

1   The Bistable Positive-Feedback Network

This section outlines a basic model for a bistable positive-feedback network. Figure 2 and Table 1 illustrate the system and the chemical equations which govern it. Essentially, the system consists of self-activated expression of a protein A and an input protein B which enzymatically degrades A.

Under the rapid equilibrium approximation we can assume that reaction (a) and (b) are in equilibrium with respect to the reactions (c) through (g). We can use the fact that there is a constant amount of total operator (O_T) to derive an equation for the free operator concentration (O) in terms of the concentration of (A). We also make use of the equilibrium equation for reaction (a) and (b).

$$(O_T) \;=\; (O) + (OA_n) = (O) + K(O)(A)^n = [1 + K(A)^n](O) \tag{1}$$

$$(O) \;=\; \frac{O_T}{1 + K(A)^n} \tag{2}$$

where K is the total equilibrium association constant $(K = (K_1 K_2)^{-1})$.

We now write an equation for the change in the concentration of (A) with respect to time using the chemical equations (c), (d), (e), and (g). We then use Equation 2 and the equilibrium equation for reactions (a) and (b) to derive $d(A)/dt$ as a function of (A) and (B).

$$\frac{d}{dt}(A) = k_{leak}(O) + k_{synth}(OA_n) - k_{AB}(A)(B) - k_{adeg}(A) \tag{3}$$

$$= k_{leak}(O) + k_{synth}K(A)^n(O) - k_{AB}(A)(B) - k_{adeg}(A) \tag{4}$$

$$= \frac{k_{leak}(O_T)}{1 + K(A)^n} + \frac{k_{synth}K(A)^n(O_T)}{1 + K(A)^n} - k_{AB}(A)(B) - k_{adeg}(A) \tag{5}$$

$$= \frac{\beta_{leak}}{1 + K(A)^n} + \frac{\beta_{synth}K(A)^n}{1 + K(A)^n} - k_{AB}(A)(B) - k_{adeg}(A) \tag{6}$$

where $\beta_{leak} = k_{leak}(O_T)$ and $\beta_{synth} = k_{synth}(O_T)$. The rate of change in A has four terms: a leakage term, a synthesis term, a enzymatic degradation term due to AB interactions, and a standard degradation term. We can use a similar analysis to derive the change in (Z) over time.

$$\frac{d}{dt}(Z) = \frac{\beta_{leak}}{1 + K(A)^n)} + \frac{\beta_{synth}K(A)^n}{1 + K(A)^n} - k_{zdeg}(Z) \tag{7}$$

The transfer curve for A versus B and Z versus B can be found by setting Equations 6 and 7 equal to zero. The resulting equation will be difficult to solve analytically for (A) or (Z) in terms of (B), but simple to solve for (B) in terms of (A) or (Z). To plot the transfer curve, one need only try a range of values for (A) to determine the corresponding input concentrations.

We will now examine the behavior of this simple positive-feedback network for a given set of parameters. Unless otherwise stated, we use the following values: $b_{leak} = 1$, $b_{synth} = 50$, $K = 10$, $k_{adeg} = 0.8$, $k_{zdeg} = 0.8$, $k_{AB} = 2$, and $n = 4$. For now our goal is to simply gain some intuition about the system, and we will use more biologically plausible parameters later in this document.

Figure 3 shows typical transfer curves for this system. Notice that for some input B concentrations there are three possible output values. We can use stability analysis to determine which of these solutions are stable and which are unstable. Figure 4 shows the vector field for $d(A)/dt$ as well as (A) versus time for several initial conditions. From this we can see that the upper and lower branches of the transfer curve are stable equilibrium points while the middle branch is clearly unstable.

Figure 5 shows two trajectories along the transfer curve. The left-hand figure shows that as (B) increases, the system moves down the upper branch until it reaches the critical point at $(B) = 25$. Here (A) sharply decreases and the system "falls off" onto the lower branch. The right-hand figure shows that as (B) decreases, the system moves back along the lower branch until it reaches the critical point at $(B) = 3$. (A) then sharply increases and the system "jumps" up on the upper branch. This illustrates the hysteresis in the system - the transfer curve is different depending upon whether we are increasing (B) or decreasing (B). We can exploit this bi-stability to create a relaxation oscillator by self-coupling the production of B to the production of A as illustrated in the following section.
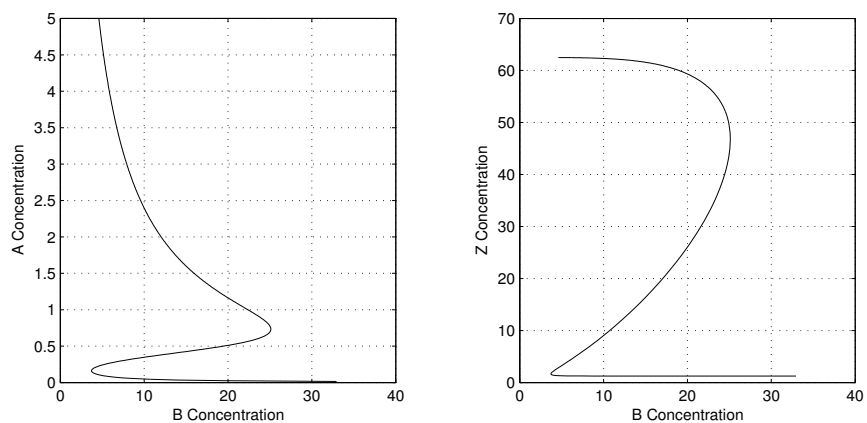
3

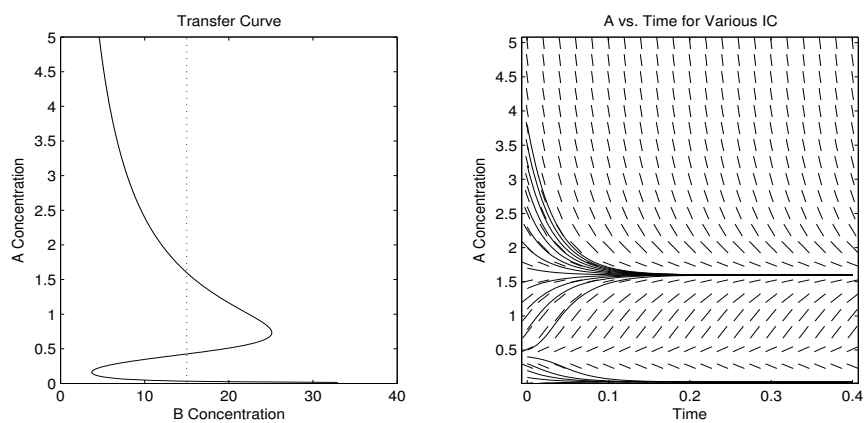Figure 3: Transfer Curves for Bistable Positive-Feedback Network.

Figure 4: Stability Analysis for Bistable Positive-Feedback Network. Dashed line on transfer curve indicates the constant input concentration of B used for the A vs time plots.
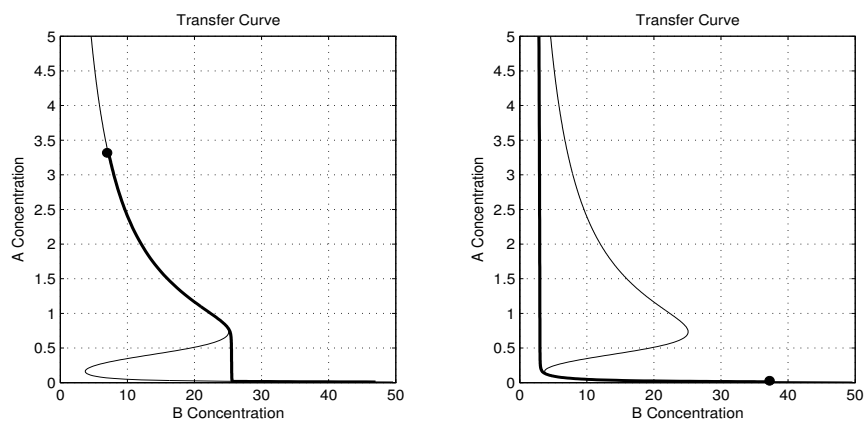

Figure 5: Transfer Curves for Bistable Positive-Feedback Network. Figure on the left is for increasing B while the figure on the right is for decreasing B.
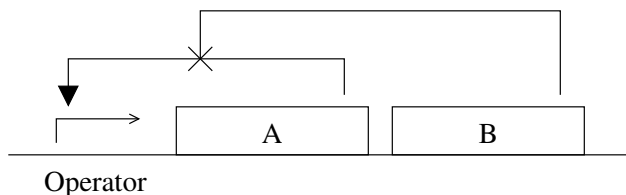
4

Figure 6: System Diagram for Simple LASRO Model

(a)	Multimerization	$nA \rightleftharpoons A_n$		$K_1 = (A)^n/(A_n)$
(b)	Activation	$O + A_n \rightleftharpoons OA_n$		$K_2 = (O)(A_n)/(OA_n)$
(c)	Leakage	$O \rightarrow O + A + Z$		k_{leak}
(d)	Synthesis	$OA_n \rightarrow OA_n + A + Z$		k_{synth}
(e)	Protein Decay	$A \rightarrow$		k_{adeg}
(f)	Protein Decay	$B \rightarrow$		k_{bdeg}
(g)	Decay of A by B	$A + B \rightarrow B$		k_{AB}

Table 2: Chemical Equations for LASRO Without Positive Feedback

2 The Relaxation Oscillator

We now self-couple the input and output of the bistable network discussed in the previous section to create the relaxation oscillator shown in Figure 6. Note that this is a greatly simplified version of the full Lux/AiiA system shown in Figure 1. Most notably, the simpler model completely ignores the difference between LuxI, HSL, and LuxR; the positive feedback is folded into a single protein A. Future work will extend the simple model to include more of the components shown in the full system. Table 2 lists the chemical equations which govern this system.

Using an analysis similar to that presented in Section 1, we can derive the following two differential equations which govern the dynamic behavior of the relaxation oscillator under the rapid equilibrium approximation.

$$\frac{d}{dt}(A) = \frac{\beta_{leak}}{1 + K(A)^n} + \frac{\beta_{synth}K(A)^n}{1 + K(A)^n} - k_{AB}(A)(B) - k_{adeg}(A) \tag{8}$$

$$\frac{d}{dt}(B) = \frac{\beta_{leak}}{1 + K(A)^n} + \frac{\beta_{synth}K(A)^n}{1 + K(A)^n} - k_{bdeg}(B) \tag{9}$$

The left-hand portion of Figure 7 shows the two nullclines for this system of differential equations. Notice that the nullcline corresponding to Equation 8 is analogous to the transfer curve shown in Figure 3. The intersection of these nullclines is the equilibrium point of the oscillator.

Figure 7 and Figure 8 also illustrate how these nullclines change when the parameters are varied. Notice that as expected changing k_{bdeg} only moves one of the nullclines, while

5

changing k_{adeg} moves the other nullcline. Changing N (ie. the cooperativity) changes both nullclines.

Figures 9, 10, and 11 show the trajectories in state space as well as the concentrations of A and B over time for several initial conditions. Notice that if the equilibrium point is on the upper or lower branch of the bistable nullcline, then the system does not oscillate but instead simply stabilizes at the equilibrium point. This is in contrast to situations where the equilibrium point is on the middle branch. Here the system will oscillate forming a limit cycle in state space regardless of the initial conditions. k_{bdeg} is varied to move the equilibrium point between the three branches.
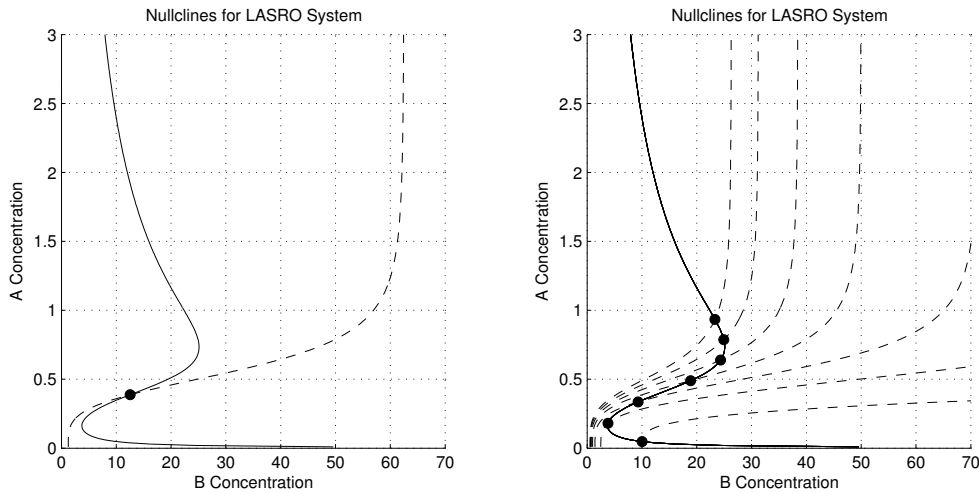

Figure 7: Nullclines for LASRO System. Left-hand figure is for the parameters used in earlier sections. Right-hand figure shows how nullclines change for $k_{bdeg} = 0.1$ to 2
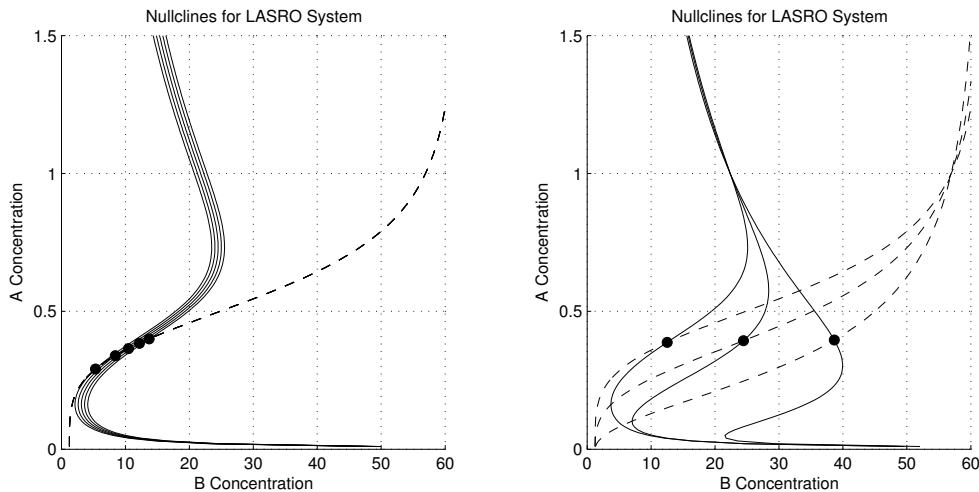

Figure 8: Nullclines for LASRO System. Left-hand figure shows how nullclines change for $k_{adeg} = 0.1$ to 4. The right-hand figure shows how the nullclines change for $n = 2$ to 4.
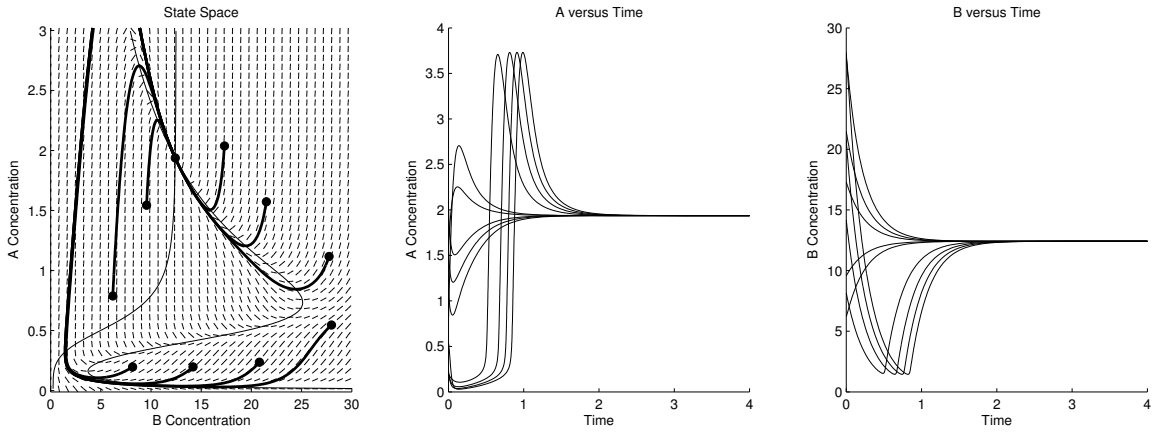
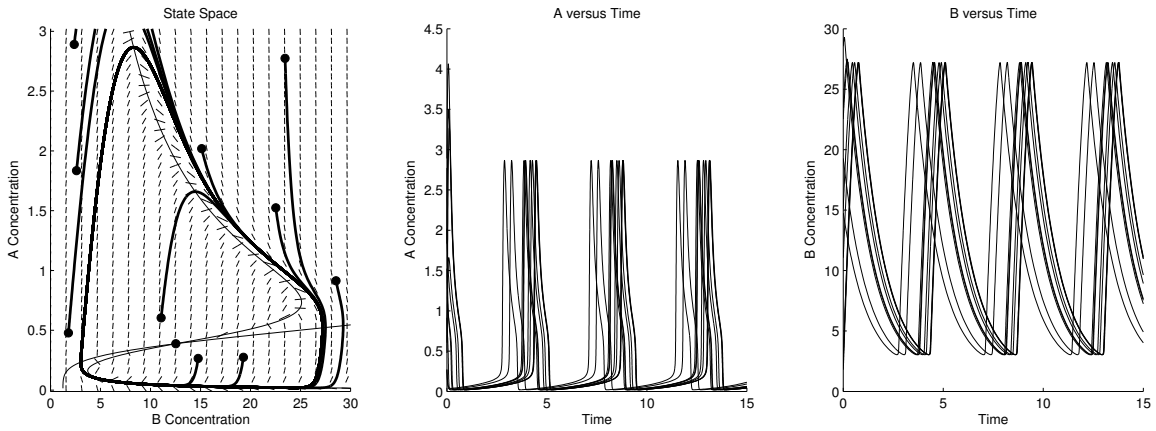Figure 9: System Dynamics when Equilibrium Point is on Upper Branch ($k_{bdeg} = 0.4$)

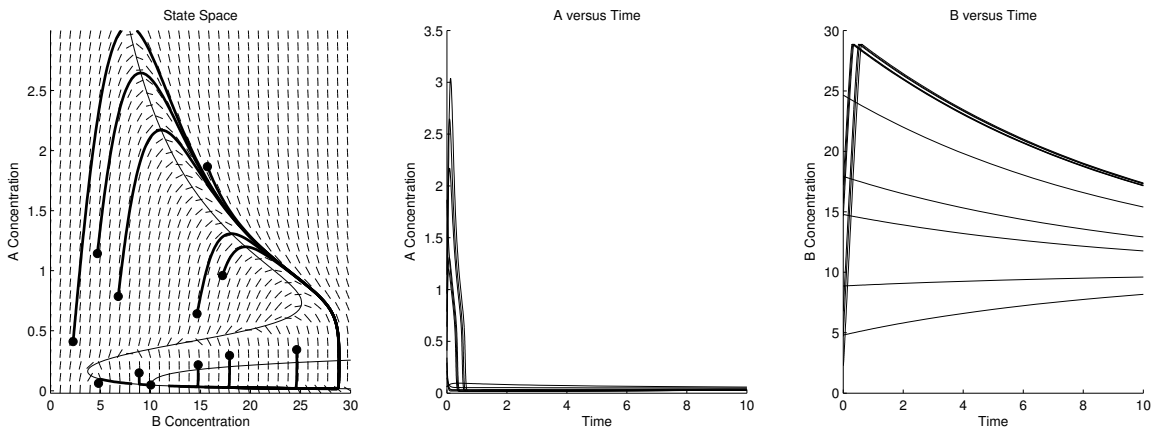Figure 10: System Dynamics when Equilibrium Point is on Middle Branch ($k_{bdeg} = 0.8$)

Figure 11: System Dynamics when Equilibrium Point is on Lower Branch ($k_{bdeg} = 0.1$)

7

3   Biologically Plausible Parameters

Our analysis so far has relied on relatively arbitrary parameter values and units. We now take a first step towards narrowing the parameter space around more biologically plausible parameters. Table 3 lists parameter values which are at least approximately on the order of what might be reasonable in biology. All concentrations are in nanomolar units (nM). We assume that the protein-protein and protein-DNA forward reactions are diffusion limited and that the reverse reactions are similar to the lambda phage system. The half-life of protein A is assumed to be around 10 minutes which is similar to what is used in Elowitz's repressilator model [1]. Furthermore, we assume that a more aggressive degradation tail can enable half-times on the order of two minutes for protein B. The enzymatic decay rate is admittedly rather arbitrary owing to the fact that the little data that is available in the literature is more applicable to the full Lux/AiiA system as opposed to the greatly simplified system studied here. Regardless, assuming that the enzymatic decay rate is twice the normal degradation rate of protein A seems reasonable. We use a hill coefficient of four; it is largely believed that the LuxR system binds as a dimer [6, 7] and we assume that the LuxR-HSL binding adds additional cooperativity [4] although this may be optimistic. Finally the fully activated synthesis rate is assumed to be on the order of a couple of proteins per second per promoter and the leakage rate is assumed to be at least two orders of magnitude less than the fully induced rate.

Figure 12 illustrates the simple LASRO system under the biologically plausible parameters listed in Table 3. The system dynamics are similar to those presented in the earlier sections. Notice the large discrepancy between the concentration range for protein A (up to 50 nM) versus protein B (up to 6500 nM). Although this is similar to the analytical results described in [2], it is still a reason for concern since such small concentrations of A (on the order of tens of proteins) could result in significant variation due to stochastic effects. The period of the oscillator is around ten minutes which seems very fast; in the next section we

| Parameter	Symbol	Value	Comment
Forward rate for multimerization	k_{a1}	0.002 $nM^{-1}s^{-1}$	Diffusion limited
Reverse rate for multimerization	k_{d1}	0.02 s^{-1}	Tighter than DNA binding
Forward rate for DNA binding	k_{a2}	0.002 $nM^{-1}s^{-1}$	Diffusion limited
Reverse rate for DNA binding	k_{d2}	0.04 s^{-1}	Similar to lambda DNA binding
Equilibrium association constant	K	0.005 nM^{-2}	$(K_1 K_2)^{-1} = (k_{a1}/k_{d1}) * (k_{a2}/k_{d2})$
Protein degradation rate of A	k_{adeg}	0.0012 s^{-1}	Half-life of 10 min
Protein degradation rate of B	k_{bdeg}	0.0058 s^{-1}	Half-life of 2 min
Enzymatic decay rate of A by B	k_{AB}	0.0024 s^{-1}	Twice as effective as k_{adeg}
Total operator concentration	(O_T)	50 nM	Medium copy count
Cooperativity	N	4	Hill coefficient
Leakage synthesis rate	k_{leak}	0.01 s^{-1}	Significantly less than k_{synth}
Fully activated synthesis rate	k_{synth}	2 s^{-1}	2 proteins per sec per plasmid copy
Leakage parameter	b_{leak}	0.5 nMs^{-1}	$k_{leak}(O_T)$
Synthesis parameter	b_{synth}	100 nMs^{-1}	$k_{synth}(O_T)$

Table 3: Biologically Plausible Parameters
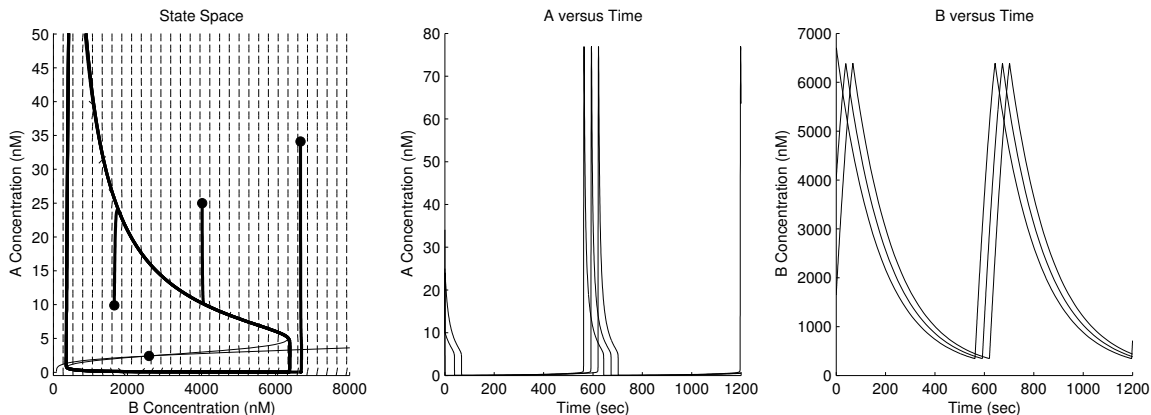
Figure 12: System Dynamics under Biologically Plausible Parameters

will show that without the rapid equilibrium approximation the system oscillates with a more reasonable period possibly suggesting that this approximation is less applicable than previously thought.

4 Revisiting the Rapid Equilibrium Approximation

Up until this point our analysis has fallen into one of two categories: (a) analytical analysis of static behavior or (b) numerical analysis of dynamic behavior under the rapid equilibrium approximation. In this section we revisit the rapid equilibrium approximation by fully simulating all of the chemical reactions without assuming that the protein-protein and protein-DNA reactions are at equilibrium. Instead we use the kinetic rate constants listed in Table 3. We simulate this system using a numerical differential equation solver for various initial conditions.

The first task is to validate the analytical static behavior described earlier in this document using the full dynamic model. These results should be similar since the static behavior is independent of the rapid equilibrium approximation (i.e. the whole system is at equilibrium). We do this by initializing the full dynamic model and then observing the concentrations of each species after a very long time period. Figure 13 compares the analytical transfer curve to the transfer curve derived from the full dynamic model for the bistable positive-feedback network introduced in Section 1. The solid line represents the analytical transfer curve while the dashed line with circle markers represents the transfer curve derived from numerical simulation. Each circle marker is the concentration of A after 24 hours of simulated time. Upper and lower branches of the numerical simulation are the result of two different initial values of (A): 100 nM and 0 nM respectively. Although similar, the transfer curve for the full dynamic model falls off the upper branch significantly earlier than the analytical model would predict. This behavior deserves further investigation, since we are unsure whether it is an artifact of the model implementation or an indication of something more significant. Regardless, the full dynamic model still exhibits the bistability necessary to make a relaxation oscillator.

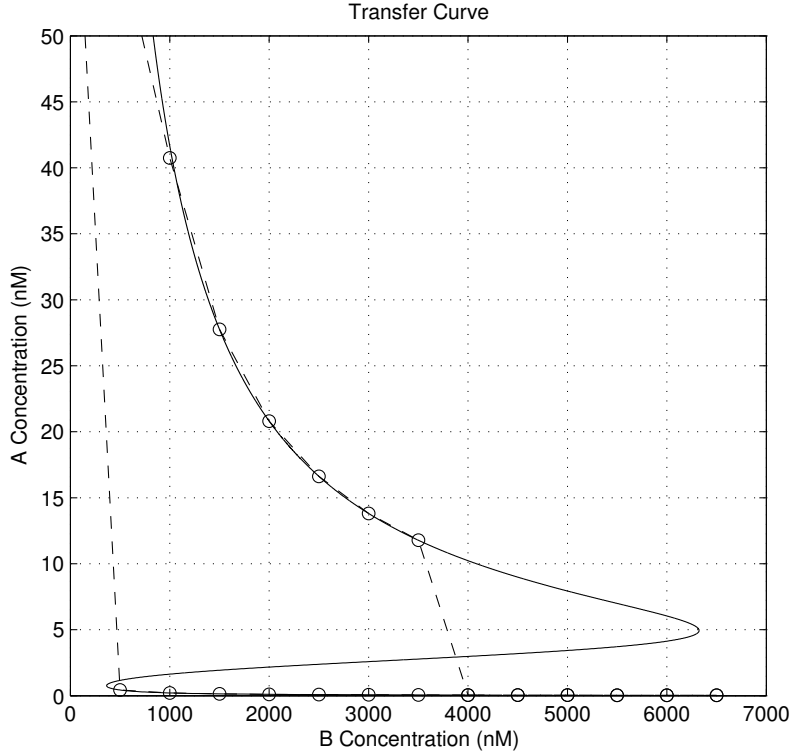Figure 14 shows the dynamic behavior of the relaxation oscillator using the full dynamic

9

Figure 13: Analytical and Numerical Transfer Curves. The solid line represents the analytical transfer curve while the dashed line with circle markers represents the transfer curve derived from numerical simulation. Upper and lower branches of the numerical simulation are the result of two different initial values of (A): 100 nM and 0 nM respectively.
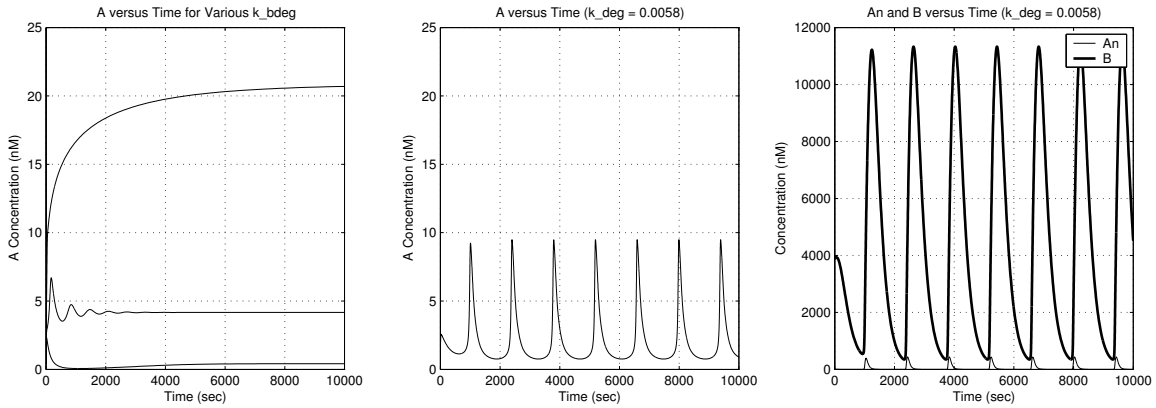

Figure 14: Oscillatory Dynamics without Rapid Equilibrium Approximation. Left-hand figure shows the concentration of A for three values of k_{bdeg} (0.05 s^{-1}, 0.01 s^{-1}, 0.001 s^{-1}) which result in a stable equilibrium point. The middle and right-hand figures show the concentration of A, A_n, and B for $k_{bdeg} = 0.0058$ s^{-1} which results in stable oscillations.
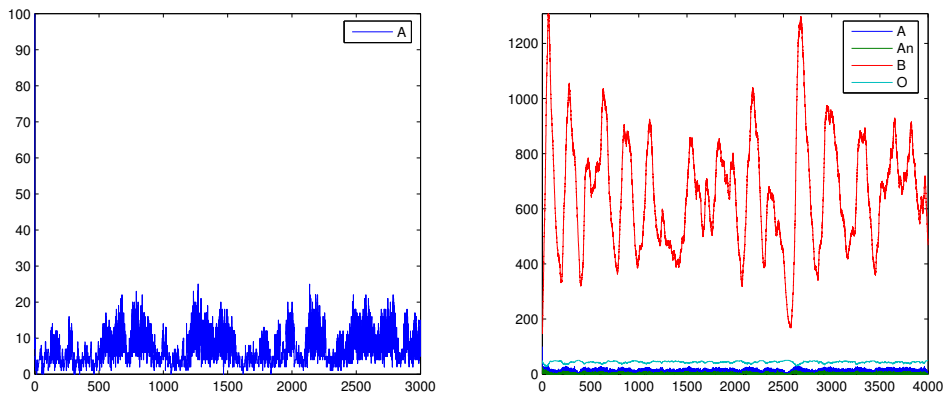
Figure 15: Oscillatory Dynamics without Rapid Equilibrium

model and the parameters given in Table 3. The left-hand figure shows the concentration of A over time for three values of k_{bdeg}. As predicted in Section 2, decreasing k_{bdeg} moves the equilibrium point down the transfer curve. For $k_{bdeg} = 0.05 \ s^{-1}$ the system stabilizes at $(A) \approx 21$ nM and thus the system is on the upper branch of the transfer curve. For $k_{bdeg} = 0.001 \ s^{-1}$ the system stabilizes at $(A) \approx 0$ nM and thus the system is on the lower branch of the transfer curve. It is peculiar that for $k_{bdeg} = 0.01 \ s^{-1}$ the system stabilizes at $(A) \approx 4$ nM, since the transfer curve derived from the full dynamic model implies that this is not a valid stable equilibrium point. Again the discrepancy in transfer curves needs further investigation.

Figure 14 also shows the dynamic behavior for $k_{bdeg} = 0.0058 \ s^{-1}$ which results in stable oscillations. This value of k_{bdeg} is between the values tested in the left-hand figure and thus we can confidently assume that the equilibrium point is on the unstable middle branch. This analysis illustrates how one can use k_{bdeg} to tune the system's equilibrium point onto the middle branch of the transfer curve and thus produce oscillations.

The period of these oscillations is around 25 minutes which is longer than what was predicted using the rapid equilibrium approximation in Section 3. This is still fast but possibly more reasonable. The discrepancy implies that the rapid equilibrium approximation may be inappropriate for this system.

5   Stochastic Modeling

Some very preliminary work has been done on modeling the relaxation oscillator using stochastic simulators such as the Stochastic Simulation Algorithm (SSA). Using such approaches one can capture the effects of discrete chemical events as opposed to the continuous models used in this document so far. Figure 15 illustrates a typical result for a stochastic simulation of the LASRO relaxation oscillator using parameters similar (but not identical) to those listed in Table 3. Notice that the quantity of A molecules fluctuates a great deal and that these fluctuations exceed the range of bistable A values in the transfer curves we have see so far. This implies that such stochastic simulation is an important step in
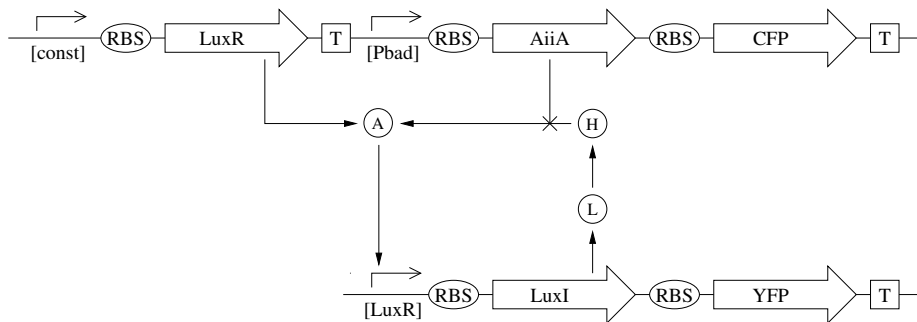
Figure 16: Test Construct for Bistable Positive-Feedback Network. L represents LuxI, H represents HSL, and A represents the full LuxR/HSL complex. The reporters do necessarily need to be polycistronic.

understanding how the relaxation oscillator will function experimentally. Even with such fluctuations, we can still observe oscillations in the amount of B. To achieve oscillations in this simulation it was necessary to add a new chemical reaction which modeled the decay of the A_n multimer complex by the B enzyme. The biological foundation for such a reaction is an important question for future work.

6 Experimental Approach

Based on the insight gained from this document, this section proposes one possible experimental approach for tuning a LASRO system to oscillate. The first step would be to construct a system similar to the bistable positive-feedback network described in Section 1 and to verify that this system has bistable behavior. Figure 16 illustrates a system which could be used to derive transfer curves similar to the one shown in Figure 13. This test construct uses the externally inducible pbad promoter to control the expression of AiiA. The transfer curves would be in terms of YFP vs CFP fluorescent units. A similar experimental approach for testing a bistable positive-feedback network was used in [3], but the actual system was very different. If there is no bistable region in this transfer curve then there is no hope of oscillations. The system can be tuned to increase the size of this bistable region and thus increase the chance of oscillations.

Armed with this transfer curve, one could then build a system similar to the relaxation oscillator shown in Figure 1. To observe the output, a YFP reporter could be added to the LuxR promoter. We would then observe the steady state amount of YFP to qualitatively judge if the oscillator is finding an equilibrium point on the upper or lower branch of the transfer curve. The degradation rate of AiiA can then be tuned using various degradation tags to move the equilibrium point onto the unstable middle branch. An important experimental question is whether there are enough degradation tags to enable the system to be fine tuned in this way.

References

[1] M. Elowitz and S. Leibler. A synthetic oscillatory network of transcriptional regulators. *Nature*, 403:335–338, 2000.

[2] J. Hasty, F. Isaacs, M. Dolnik, D. McMillen, and J. Collins. Designer gene networks: Towards fundamental cellular control. *CHAOS*, 11(1):207–220, 2001.

[3] F. Isaacs, J. Hasty, C. Cantor, and J. Collins. Prediction and measurement of an autoregulatory genetic module. *PNAS*, 100(13):7714–7719, 2003.

[4] D. McMillen, N. Kopell, J. Hasty, and J. Collins. Synchronizing genetic relaxation oscillators by intercell signaling. *PNAS*, 99(2):679–684, 2002.

[5] Modified barkai-leibler relaxation oscillator. California Institute of Technology synthetic biology team report: http://www.cds.caltech.edu/~rwald/sbc04/, 2004.

[6] A. Vannini, C. Volpari, C. Gargioli, E. Muraglia, R. Cortese, R. D. Francesco, P. Neddermann, and S. D. Marco. The crystal stucture of the quorum sensing protein trar bound to its autoinducer and target dna. *The EMBO Journal*, 21(17):4393–4401, 2002.

[7] M. Welch, D. E. Todd, N. A. Whitehead, S. J. McGowan, B. W. Bycroft, and G. P. Salmonda. N-acyl homoserine lactone binding to the carr receptor determines quorum-sensing specificity in erwinia. *The EMBO Journal*, 19(4):631–641, 2000.